Research Article

Evaluation of thermal degradation and melt crystallization behavior of taro mucilage and its graft copolymer with poly(lactide)

Abubakar Hamisu Mijinyawa[1] · **Geeta Durga**[1] · **Anuradha Mishra**[2]

Received: 23 April 2019 / Accepted: 12 October 2019 / Published online: 25 October 2019
© Springer Nature Switzerland AG 2019

Abstract
This communication presents the thermal degradation behavior and non-isothermal crystallization kinetics of taro mucilage (CEM) and its graft copolymer polylactide (CEM-g-PLA) by thermogravimetric analysis (TGA/DTG coupled techniques) and differential scanning calorimetric. Isoconversional degradation analysis for CEM and CEM-g-PLA performed with the aid of Friedman, Kissinger (KSS), Flynn–Wall–Ozawa (FWO), and Kissinger–Akahira–Sunose (KAS) methods. The energy profiles and Criado plots over specific conversion (α) were able to predict that both CEM-g-PLA and CEM followed multi step kinetics and different degradation mechanisms. The Ozawa model fitted the melt crystallization data for CEM-g-PLA and its exponent (m) complements those for the modified Avrami and Tobin models. The crystallization of CEM-g-PLA was characterized with the formation of two distinct crystal growths. Further, the negative isoconversional activation energy suggested the occurrence of melt crystallization in CEM-g-PLA. Thus, the grafting of PLA onto CEM resulted into a material that shows thermal properties entirely different from that of its precursor (CEM) besides having an increased shelf life and not compromising with biodegradability. The analyzed data from the isoconversional equations (viz. Friedman, FWO and KAS models) and Ozawa model could be useful in modelling the degradation stability/mechanism and crystallization behavior of polylactide-grafted copolymer.

Keywords Taro mucilage · Poly(lactide) · Grafted copolymer · Isoconversional analysis · Melt crystallization

1 Introduction

By virtue of having good film forming and barrier properties against the gases specifically oxygen and carbon dioxide, natural polysaccharides have made their place as an alternative to synthetic polymers in the field of food packaging [6, 9]. Their mechanical and thermal properties and shelf life can be tailor-made by blending different polysaccharides or by grafting biodegradable and biocompatible synthetic polymer such as polylactide [17].

Polylactide or polylactic acid (PLA) is a renewable and biodegradable thermoplastic polyester [2] and a potential candidate for grafting/blending with polysaccharide. Most common ways of grafting PLA onto natural polysaccharide are through direct polycondenzation and ring opening polymerization methods [16, 27]. There are many conventional ways to prepare graft copolymers but the literature recommends grafting under commercial microwave because of its better heating effect, ease of control of parameters, and drastic reduction of grafting time [26, 31]. Despite the diverse nature and structure of the classical

Electronic supplementary material The online version of this article (https://doi.org/10.1007/s42452-019-1490-4) contains supplementary material, which is available to authorized users.

✉ Anuradha Mishra, anuradha_mishra@rediffmail.com | [1]Department of Chemistry, Sharda University, Greater Noida, Uttar Pradesh 201306, India. [2]Department of Applied Chemistry, School of Vocational Studies and Applied Sciences, Gautam Buddha University, Greater Noida, Uttar Pradesh 201312, India.

polysaccharide biomaterials and the biocompatible and biodegradable nature of PLA, not many reports on the synthesis and characterization of PLA-grafted polysaccharides have been in scientific literature. These graft copolymers have potential applications in plastics, biomedical, pharmaceuticals and food Industries.

The knowledge of thermal analysis of any material is useful to decide its potential industrial applications. Knowing the thermal degradation patterns and parameters could help to predict the lifetime/thermal stability of a material [24]. Moreover, isoconversional analysis of polymeric materials [3, 15] have seen novel applications in the areas of the glass transition and polymer melt crystallization [32]. The non-isothermal crystallization kinetics is also of great importance for it is directly or indirectly relates to the physical and mechanical properties of the polymer [18].

Many polysaccharides can be grafted with polylactic acid to make them more useful material for various industrial applications. In the present study, we have explored the thermal degradation behavior and crystallization kinetics of taro mucilage and its polylactide-grafted copolymer (CEM-g-PLA) by using the thermogravimetric analysis (TGA) and differential scanning calorimetric (DSC) under non-isothermal conditions. The results obtained for CEM-g-PLA and CEM were compared to understand the effect of PLA grafting on thermal properties of the taro mucilage. After doing a thorough literature survey and to the best of our knowledge, there is no any publication reported elsewhere describing comprehensively the thermal analysis of the CEM-g-PLA.

2 Materials and methods

2.1 Materials

The CEM-g-PLA copolymer (Grafting%, and Grafting Efficiency% = 133.0 and 33.3, respectively) was synthesized under commercial microwave oven via ROP of lactide (LA) onto taro mucilage (CEM) backbone chain catalyzed by stannous octoate using chloroform as solvent. The full details of the isolation of the CEM and synthesis of CEM-g-PLA have been published earlier by our group [22]. The graft chain length of the copolymer was 100 as determined by analysis of its ^{1}H NMR spectrum (Fig. S1) using the integral intensity ratio method [19].

2.2 Thermogravimetric analysis (TGA)

Thermal degradation behavior of both CEM and CEM-g-PLA copolymer explored using TGA Q-500 (TA instrument, USA) analyzer. Samples (size: 12–13 mg) placed on platinum crucible and heated from RT (room temp.) to 600 °C, on heating rates of 4–20 °C/min and under inert nitrogen atmosphere (flow rate 60 ml/min).

2.3 Differential scanning calorimetry (DSC)

DSC study with the help of DSCQ-200 (TA instrument, USA) has been carried out to get information on the thermal transitions occurring within the materials in the course of heating under an inert nitrogen atmosphere. The specimen samples were placed on aluminum pan and then subjected to heating cycle from RT to 140 °C at a constant heating rate of 10 °C/min and held isothermally for 5 min. Then, the samples were cooled to the room temperature until the crystallization process completed at constant cooling rates of 10, 15, and 20 °C/min, respectively. The exothermic crystallization DSC peaks recorded as function of time at particular temperature to determine the relative crystallinity, X_c (t)-a parameter useful for the crystallization kinetics investigations.

2.4 Thermal isoconversional degradation behavior of CEM and CEM-g-PLA

2.4.1 Theoretical background

All kinetic degradation TGA experiments investigated using the general fundamental rate equation described as follows [5]

$$\frac{d\alpha}{dt} = kf(\alpha) \tag{1}$$

where k and f(α) are rate constant and reaction model, respectively and α denotes the extent of conversion and is expressed as

$$\alpha = \frac{W_o - W_t}{W_o - W_f} \tag{2}$$

where W_o is initial weight of sample; W_t is sample weight at time t for a given temperature, and W_f is final weight of sample.

For dynamic TGA kinetic analysis, the following basic equation is used for determining the kinetic parameters including the apparent activation energy (E_a)

$$\frac{d\alpha}{dT} = (A/\beta)\exp\left[-E_a/RT\right]f(\alpha) \tag{3}$$

where E_a is apparent activation energy, A is pre-exponential factor, β is the heating rate, R and T are gas constant (8.314 J/K mol) and Kelvin temperature, respectively.

2.4.2 Thermal isoconversional analysis

The isoconversional methods allow the determination of apparent activation energy (E_a) under different extent of conversion (α) without prior knowledge on the reaction mechanism. Further, the isoconversional methods are better than model-fitting approach, which is usually criticized for its unreliability towards the computation of the Arrhenius activation energy (E) parameter. The most familiar and widely established model-free methods include the Friedman (F), Kissinger (KSS), Flynn–Wall–Ozawa (FWO), and Kissinger–Akahira–Sunose (KAS) methods, which are usually applied for the calculation of Arrhenius activation energy under the different heating rates [8, 10, 20, 23]. The details about the description and linear expressions (Eq.S1–S4) of each of the respective models are provided separately in the supporting information section.

2.5 Non-isothermal melt-crystallization kinetics of CEM-g-PLA

During the DSC tests, heat flow can be measured as a function of time or temperature. In this study, the crystallization of CEM-g-PLA studied from its molten state referred to as the melt crystallization kinetics. The relative crystallinity, X_c (t) of CEM-g-PLA at crystallization time (t) determined by integrating the DSC exotherms from the starting to the end time of crystallization. Thus, the X_c (t) is expressed as

$$X_c(t) = \frac{\int_{t_s}^{t} \left(\frac{dH}{dt}\right) dt}{\int_{t_s}^{t_e} \left(\frac{dH}{dt}\right) dt} \quad (4)$$

where t_s and t_e represent the start/onset and end melt crystallization time.

Crystallization half time ($t_{1/2}$), is an important parameter for predicting the rate of crystallization in polymers. It is the time require by the polymeric sample for 50% crystallization [37]. The non-isothermal melt crystallization of CEM-g-PLA under three different cooling rates was explored with the help of the Avrami, Ozawa and Tobin model equations (Eq. S5 to Eq. S7). The linear equations of each of the model are given in the supporting information section. Now, Eq. S5 (a modified form of the Avrami model), is applicable for the non-isothermal crystalization [29]. The relative crystallinity below 20% has been considered for the verification of the Avrami model.

2.6 Mechanism for the melt crystallization in CEM-g-PLA

The activation energy for the melt crystallization in polymer is dependent upon temperature [12]. The mechanism for the melt crystallization in CEM-g-PLA under non-isothermal condition can be explained by examining the variation of the activation energy (E) with temperature (T). The melt crystallization DSC data is treated as per the isoconversional Friedman differential method according to the Eq. S1. Here, the conversion factor 'α' was taken as fractional area under the DSC curves obtained for the crystallization, and the 'α' values chosen ranged from 0.2 to 0.7 due to good fitting. The dependence of 'E_α' on 'α' was obtained from the isoconversional method, and then it was transformed into 'E_α versus T' by replacing α with the mean temperatures under different cooling rates [34].

3 Results and discussion

3.1 Thermal degradation behavior of CEM and CEM-g-PLA copolymer

Thermogravimetric analysis under inert nitrogen atmosphere and at heating rates of 10, 15, and 20 °C/min were used to study the thermal degradation behavior for CEM and CEM-g-PLA copolymer. The TG/DTG curves of samples displayed distinct differences in terms of the absorbed water content, number of degradation stages, and residual weight. On the TG/DTG curves (Fig. 1a, b) of CEM, three degradation stages were noticeable for the heating rates 10 °C/min only, and for 15 °C/min and 20 °C/min, the second stage showed almost negligible shoulder due to increased heating effects. The weight loss below 100 °C represented the dehydration of absorbed water/moisture. Second weight loss between 100 and 150 °C (at heating rate 10 °C/min) appeared as small signal and it could be due to the denaturing of the amorphous part of CEM. Large signals on the DTG curves of the CEM were visible at 272.9–279.1 °C with significant weight loss (69.4–64.9%). These signals corresponded to the structural decomposition of natural taro mucilage [28]. At 600 °C temperature, 24.1–17.1% residues obtained for the heating rates 10–20 °C/min.

Figure 1c, d shows the TGA/DTG of CEM-g-PLA copolymer under different heating rates. Thermal behavior of the copolymer was different from that of the mucilage due to the incorporation of low thermally stable PLA chains. The CEM-g-PLA exhibited two major degradation stages. The major degradation stages occurred between 150 and 200 °C (i.e. corresponding to 163.3, 167.0, and 174.7 °C) with significant weight losses of 84.0%, 72.1%, and 71.7%.

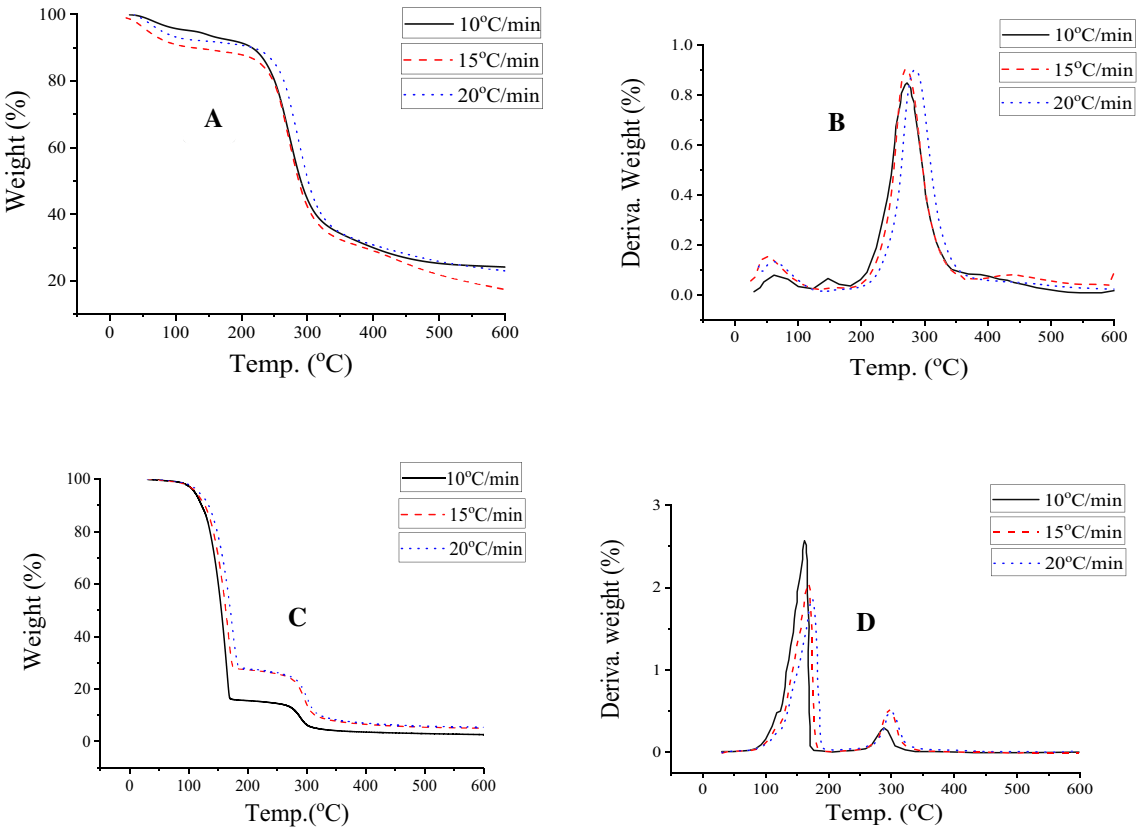

Fig. 1 TG/DTG curves for CEM (**a** and **b**) and CEM-g-PLA copolymer (**c** and **d**) at10 °C/min, 15 °C/min, and 20 °C/min heating rates

The thermal stage over the temperature range represented the decomposition of the PLA portion of the CEM-g-PLA copolymer [22] and has confirmed the formation of the copolymer. It was inferred that the CEM portions of the copolymer were stable at 290.1–300.28 °C at various heating rates. At 600 °C, the residual weight losses in the CEM-g-PLA were ranged between 2.6 and 5.5%. The major degradation of CEM-g-PLA was due to the grafted PLA, and the corresponding temperature was lower than for previous reports [14, 36]. The high content of grafted PLA chains might have resulted a two-step degradation steps/or derivative TG peaks [13] for the CEM-g-PLA whereby it's PLA and CEM components exhibited low and high degradation temperatures, respectively. Other reasons that could have contributed to the low degradation temperature of the grafted PLA in copolymer are the possibility of existence of some weak hydrogen interactions between the PLA and CEM and its self the PLA has low thermal degradation stability [21]. However, the degradation temperature of the PLA in the CEM-g-PLA was even higher than the one reported in the literature [19].

To validate the degradation behaviors for the CEM and CEM-g-PLA, the degradation experiments were carried out at the heating rates 4–8 °C/min (Fig. S2). The natures of the thermal degradation curves shown certain resemblance to those under higher heating rates and the maximum decomposition temperatures under the low heating rates corresponded within the range (i.e. 150–200 °C for PLA in the CEM-g-PLA and 250 –300 °C for CEM). For the materials under this study, the results from the two different heating rates were comparable and could provide similar thermal degradation mechanisms.

3.2 Thermal isoconversional degradation analysis of CEM and CEM-g-PLA

The thermal degradation behaviors of CEM and CEM-g-PLA grafted copolymer investigated using the different isoconversional models under nitrogen atmosphere and non-isothermal conditions at heating rates of 10–20 °C/min have been discussed in this section. Figures 2 and 3 show the isoconversional Friedman (A) and KSS (B and C) for CEM and the Friedman (A), KSS (B and E) FWO (C), and KAS (D) plots for the corresponding CEM-g-PLA copolymer. The Arrhenius activation energy (E_α) for the thermal degradation of CEM and CEM-g-PLA was determined from the slope of the linear plots for each kinetic model. Figure 4 shows the energy profile curves for CEM (Fig. 4a–c)

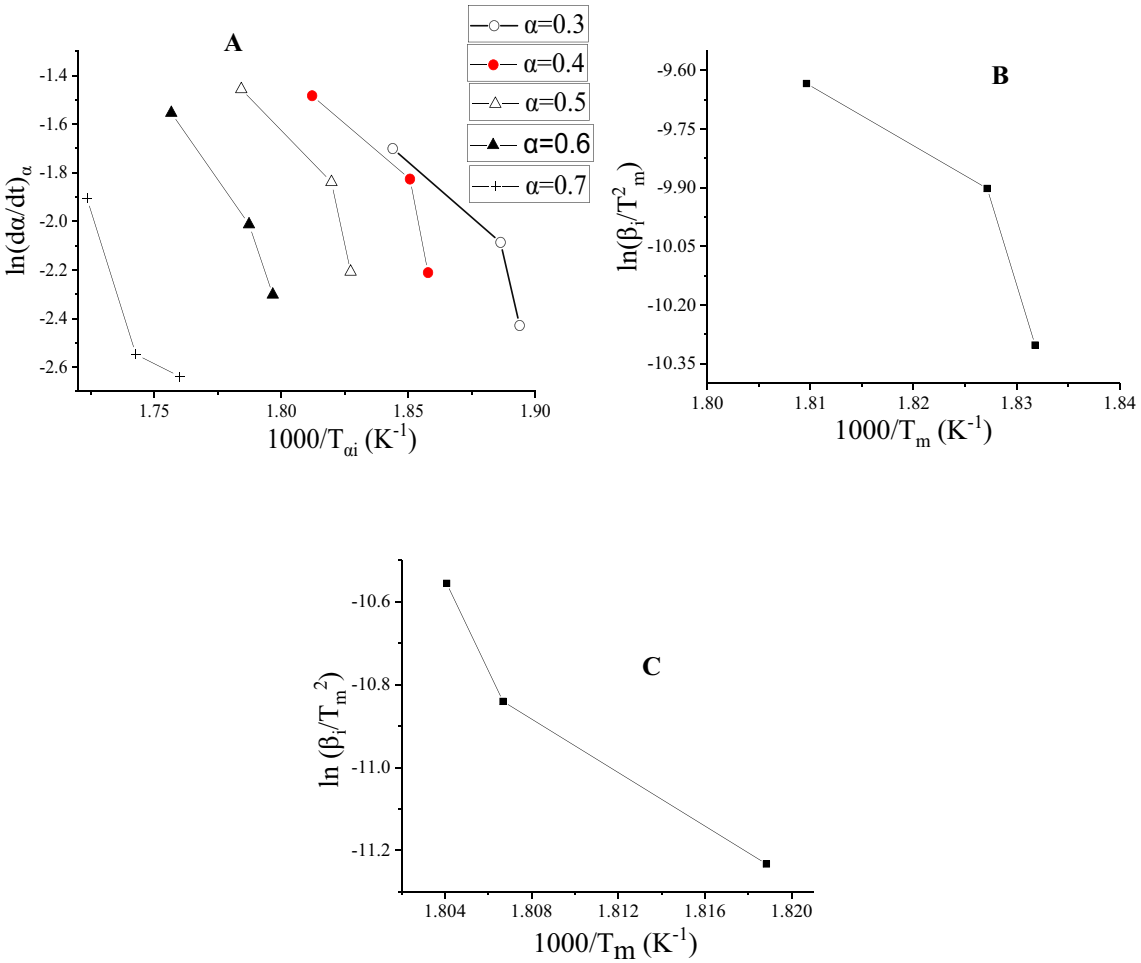

Fig. 2 The isoconversional Friedman (**a**) and KSS (**b** and **c**) plots for CEM. *Note*: 1) Each of the linear line plots (**a**), was generated using these heating rates: 10 °C/min, 15 °C/min, and 20 °C/min over the range α = 0.3–0.7; 2). **c** KSS plot obtained at the rates of 4–8 °C/min)

and CEM-g-PLA (Fig. 4d–f), representing dependence of E_α on α, taking $(d\alpha/dt)_\alpha$ versus T as reference for experiment conducted at 20 °C/min for the purpose of clarity. The Friedman degradation kinetic analysis for CEM at extent of conversion, α = 0.3–0.7 (calculated using Eq. (1)) selected since at low and high conversions, kinetic experimental curves display more deviations while in case of CEM-g-PLA copolymer, the conversion (α) values limited in the range 0.1–0.7.

The calculated squares of correlation coefficient (R^2) obtained from Friedman plots for CEM ranged from 84.0 to 97.2% (Fig. 2a). It was noticeable that over the conversions, α = 0.3–0.7, this studied model could suitably describe the degradation kinetics of CEM due to its good fitting to the degradation data. The activation energy (E_α) for degradation of CEM at conversion, α = 0.3–0.7, from Friedman model were computed to be 105.6 kJ/mol, 113.1 kJ/mol, 127.6 kJ/mol, 147.9 kJ/mol, 168.9 kJ/mol, respectively. The increased activation energy with increasing conversions (Fig. 4a) as obtained from Friedman model suggested that thermal decomposition of CEM preceded via a complex reaction mechanism. The Friedman method is therefore an applicable model to the degradation study of CEM. At temperature below 100 °C, moisture content was removed from the CEM at conversion between α = 0.3 and 0.4 which needed lower energy, and the major degradation that occurred below 300 °C at conversion between α = 0.5 and 0.6 needed significantly higher activation energy. The Arrhenius single activation energy deducted from Kissinger, KSS (R^2: 82.1%) model was found to be 216.8 kJ/mol, which is the maximum energy required for bond breakage of the structural unit of CEM.

The Friedman (A), KSS (B and E), FWO (C) and KAS (D) plots for degradation process in CEM-g-PLA are shown in Fig. 3. The squares of the correlation coefficients (R^2) for Friedman, FWO, and KAS methods over the conversion (α = 0.1–0.7) were determined as 95.9–98.9%, 96.8–99.1%, and 96.1–98.7%, respectively. In this case, there existed

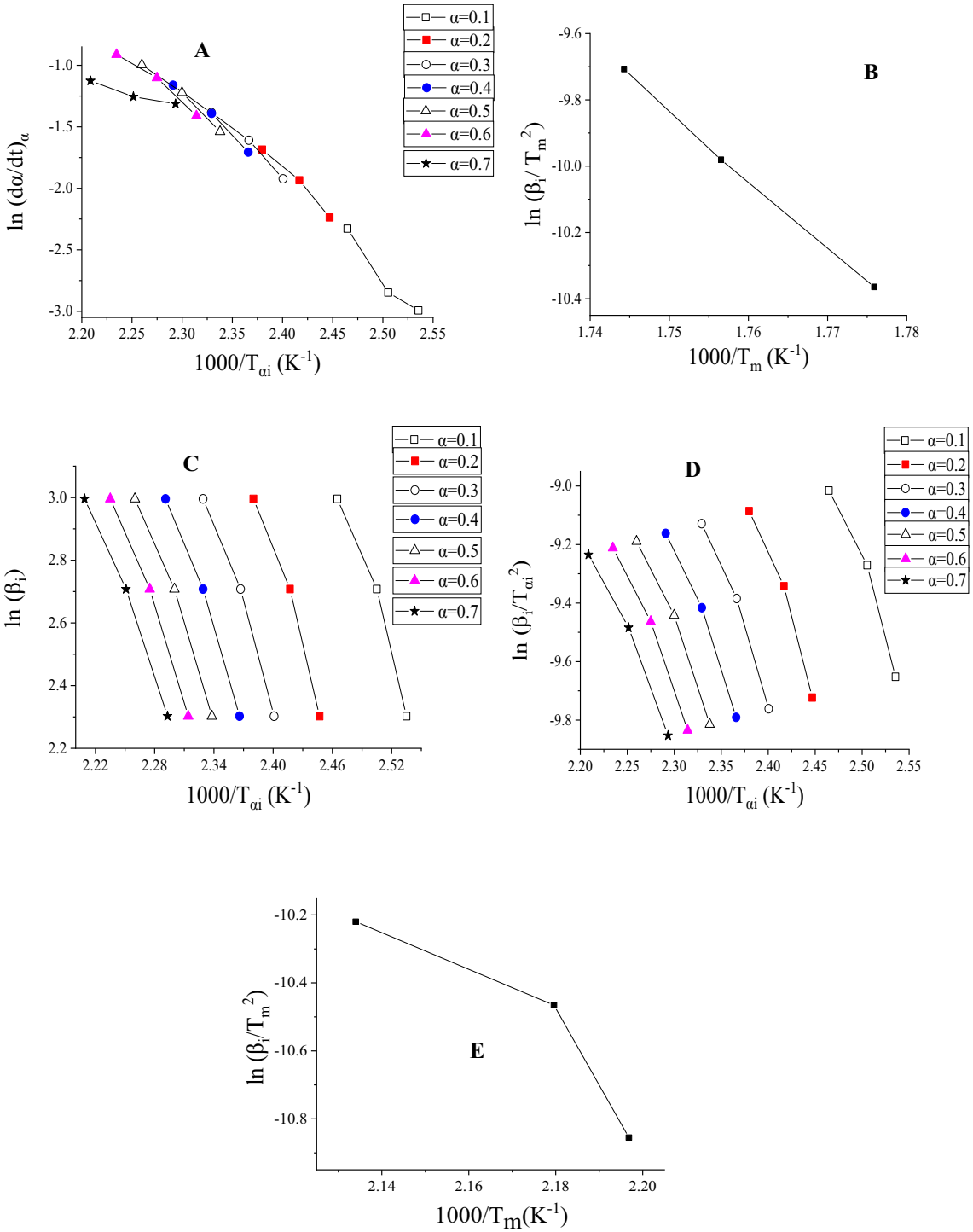

Fig. 3 The isoconversional Friedman (**a**), KSS (**b** and **e**), FWO (**c**), and KAS (**d**) plots for CEM-g-PLA copolymer. *Note*: 1) Each of the linear line plots (in **a**, **c**, and **d**), was generated at heating rates: 10 °C/min, 15 °C/min, and 20 °C/min over the range α = 0.1–0.7; 2). **e** KSS plot obtained at the rates of 4–8 °C/min)

improved statistical fitting of these models to the TGA data for all conversions in comparison to that of CEM. This further allowed the evaluation for values of the apparent activation energy (E_α) using Eq. (S1), Eq. (S3), and Eq. (S4). Their corresponding activation energies over the conversion range (α = 0.1–0.7) were computed to be 18.4–79.8 kJ/mol, 65.2–77.1 kJ/mol and 65.0–77.9 kJ/mol, respectively. Thus, the thermal degradation of CEM-g-PLA required

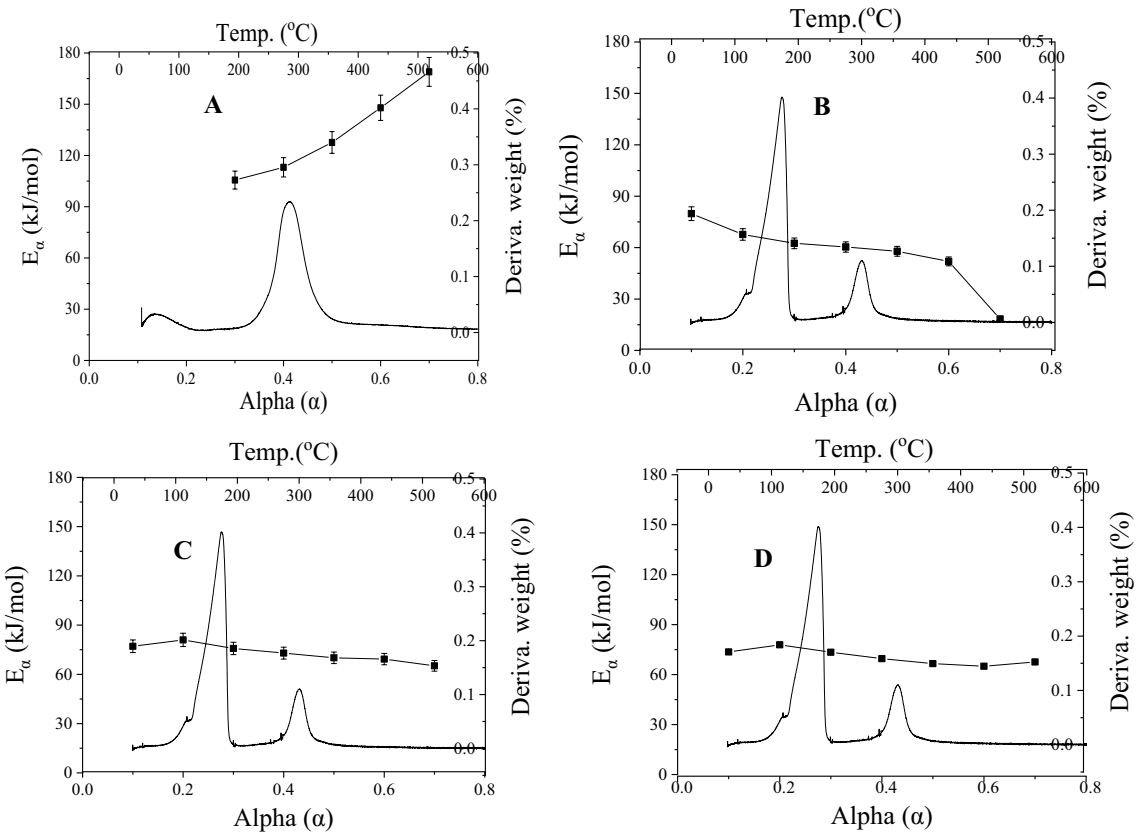

Fig. 4 Dependence of the activation energy (E_α) on the conversion degree (α) for non-isothermal degradation of CEM obtained by the Friedman (**a**) model and for CEM-g-PLA copolymer by the Friedman (**b**), FWO (**c**) and KAS (**d**)

lower activation energies at all conversions as compared to those of CEM. This could be attributed to the presence of weakly bonded ester linkages (–C–O–C=O bond) in CEM-g-PLA copolymer [22]. In CEM-g-PLA copolymer, the dependence of the activation energy (E_α) over α has been attributed to two main degradation regions for the three models (Fig. 4b–d).

The initial degradation stage in CEM-g-PLA required higher activation energy at lower conversion (0.1–0.2) than that found for the last stage. According to the molecular theory of collision [35], molecules must possess sufficient amount of kinetic energy before they can collide to initiate certain chemical reaction. Subsequently, the interatomic bonds are weaken and leading to bond cleavage during the thermal event. In case of CEM-g-PLA, the major degradation of the copolymer occurred between 150 and 200 °C at conversion near around α = 0.3, which represented the degradation of grafted PLA chain. The second region possessed low energy of activation and its DTG peak temperature shifted slightly above 300 °C at conversion between α = 0.4 and 0.5, which stood for degradation of CEM portion in grafted copolymer. Since the energy of activation (E_α) for degradation of the CEM-g-PLA varied throughout the conversion range (α = 0.1–0.7), the thermal degradation of CEM-g-PLA could be designated as a reaction having complex mechanism. The activation energy from KSS model (R^2: 99.9%) was found to be 172.2 kJ/mol, which was lower than that required for the degradation of CEM due to the weakly bonded ester linkages in CEM-g-PLA.

The described degradation kinetics above for the CEM and CEM-g-PLA was compared with thermal experiments obtained under the low heating rates i.e. 4–8 °C/min. From Fig. S3 and S4, the slopes of the isoconversional plots were all positive, and their magnitudes when multiplied with the negative terms of the slopes in Eq. S1–Eq. S4, produced negative activation energy. This observation excluded the applicability of KSS model (Figs. 2c, 3b) that determined the precise positive value of the activation energy. The plots for the KSS models in the Figs. 2 and 3 appeared with negative slopes under all the heating rates. Thus, under the low heating rates, despite their comparatively good linear fitting, out of the analyzed isoconversional methods, only the KSS model could determine accurately the degradation activation energy in CEM and CEM-g-PLA with positive values.

Criado method [1, 7] was adopted to determine further the various degradation mechanisms that might be involved during the decomposition process of CEM and its polylactide-grafted copolymer. The calculated E(α) values for the CEM and CEM-g-PLA obtained from the KSS model facilitated the preparation of the Criado experimental curves (Fig. 5b), which were then compared with master plots (Fig. 5a) for different solid-state kinetic degradation models as described by Sergey et al. [30]. The plots of Z (α) against α produced the master plots and experimental curves [5]. The shapes of the experimental curves (Fig. 5b) for degradation at 20 °C/min was compared with those of the corresponding master plots (Fig. 5a), to predict precisely the kind of degradation mechanisms taking place in CEM and CEM-g-PLA. In CEM, at conversion α = 0.1–0.4, the degradation seemed to have R2 and R3 mechanisms. The degradation shifted to Mampel first order (F1) and Avrami-Erofeev (A2, A3, and A4) type reaction mechanisms at conversion between α = 0.5 and 0.6. Similarly, for CEM-g-PLA the Criado experimental curve resembled the master plots for a two-dimensional diffusion (D2) mechanism within the conversion range α = 0.1–0.6. The conversions α = 0.2–0.5 contained straight lines similar to those for one-dimensional diffusion (D1) and the power laws (P2/3, P2, P3, and P4) degradation mechanisms. These findings suggested that the thermal degradation mechanisms for CEM and CEM-g-PLA polymers are entirely dissimilar at the specified conversions.

3.3 Melt crystallization kinetics for CEM-g-PLA

Figure 6 shows the DSC scans for CEM, CEM-g-PLA obtained through simultaneous heating, and cooling phases at various cooling rates to evaluate melt crystallization kinetics of the polymers. The CEM failed to crystallize under all cooling rates (Fig. 6a), possibly due to its highly restricted molecular chain mobility. Contrarily, the flexibility of PLA chains in CEM-g-PLA could have provided the copolymer an increased freedom for molecular motion, hence easily crystallizable. Thus, the crystallization study

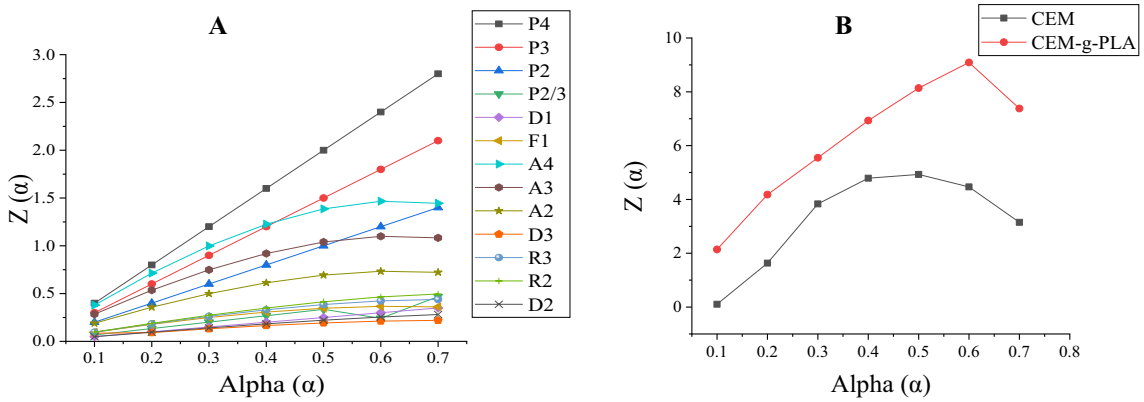

Fig. 5 **a** Master plots for different solid-state degradation mechanisms. **b** Experimental curves for degradation of CEM and CEM-g-PLA

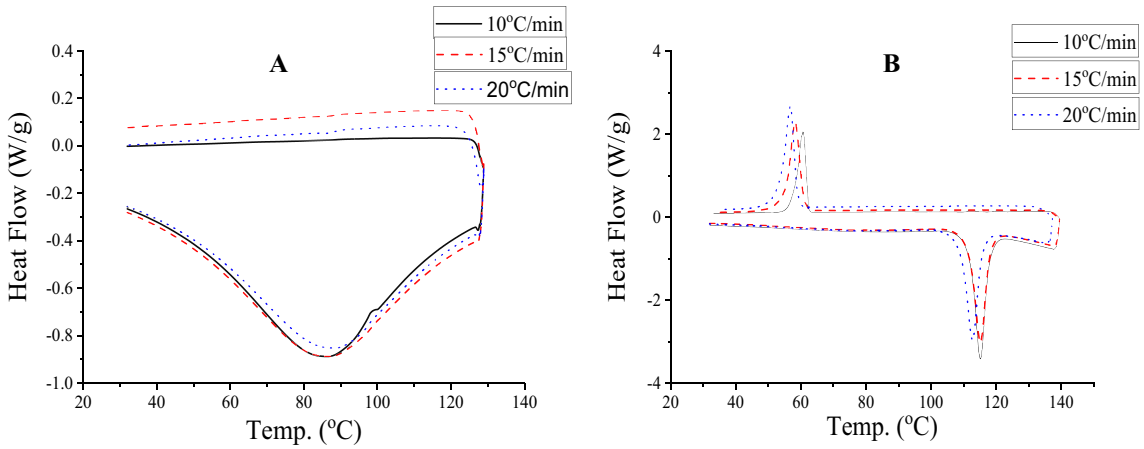

Fig. 6 DSC scans for **a** CEM and **b** CEM-g-PLA (heating rate 10 °C/min, cooling rate 10–20 °C/min)

was done only for the CEM-g-PLA copolymer. The melt-crystallization usually proceeds by cooling the melted polymer to form crystals at specific crystallization temperature [11]. Hence, the crystallization of PLA in CEM-g-PLA would occur at low temperature downwards below its melting curve unlike cold-crystallization that proceeds above glass transition temperature. It was observed that the crystallization enthalpy (ΔH_c: 43.2–34.7 J/g) and crystallization peak temperatures (T_{cp}: 60.94–57.17 °C) for CEM-g-PLA decreased when cooling rates increased from 10 °C/min to 20 °C/min (Fig. 6b). The grafted PLA (contained in the CEM-g-PLA) enhanced crystallization through its nucleation ability. Further, the appearance of strong exothermic peak of PLA exhibited an effect by further shifting the crystallization temperature to low value along the cooling curves of the CEM-g-PLA. Thus, the crystallinity of CEM-g-PLA reached its maximum at both lower temperatures and at cooling. The relative crystallinity plots for CEM-g-PLA for the different cooling rates are shown in Fig. 7. It was apparent from the plots that the overall crystallization time at 10 °C/min and at 15 °C/min was 1.10 min and 1.08 min, respectively. At 20 °C/min, the time reduced further to 0.86 min as expected. The Crystallization half time ($t_{1/2}$) found to be 0.6 min, 0.5 min and 0.4 min as the cooling rates changed from 10 to 20 °C/min.

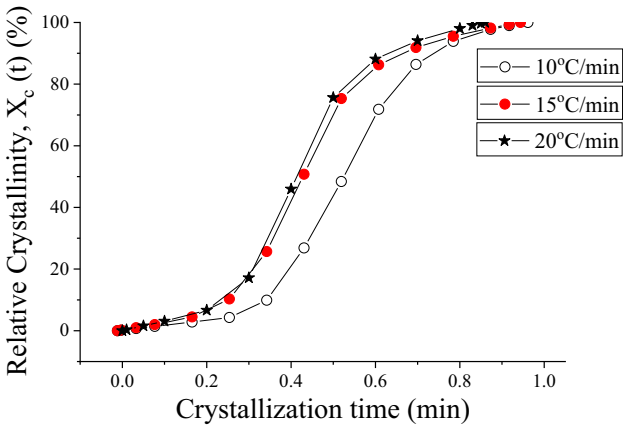

Fig. 7 Relative crystallization, X_C (t) plots for CEM-g-PLA under cooling rates of 10–20 °C/min

The Avrami, Ozawa, and Tobin plots for the crystallization kinetics of CEM-g-PLA are depicted in Fig. 8. For clear understanding of the crystallization process in CEM-g-PLA, the values of the parameters such as Avrami exponent 'n', crystallization rate constant, Ozawa exponent 'm' or simply 'n', and Tobin exponent 'n_T' were determined from their respective slope and intercept of the linearized regions of the plots. The modified Avrami plots for CEM-g-PLA under the different cooling rates were similar and each graph characterized by one linear dependence region (Fig. 8a), suggesting that there existed one kinds of crystal growth rates occurring at low crystalline domains (below 20% crystallinity). The Tobin plots (Fig. 8c) revealing crystal growths at both

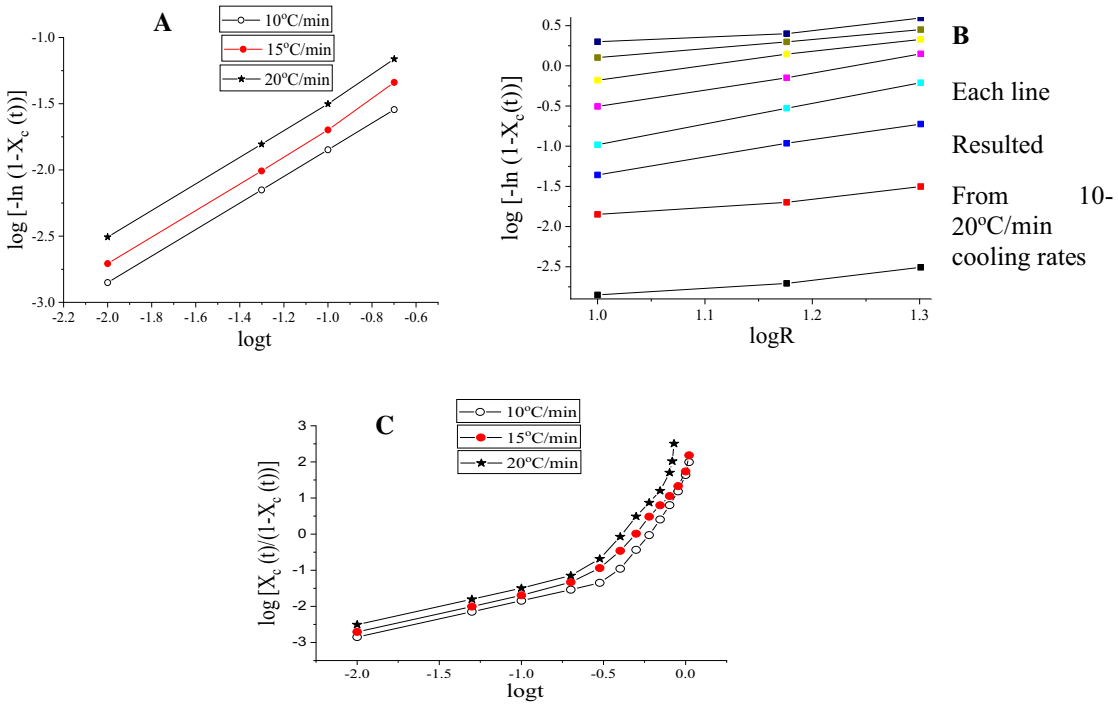

Fig. 8 The Avrami (**a**), Ozawa (**b**), and Tobin (**c**) model plots each generated at cooling rates of 10–20 °C/min

low and crystalline regions showed two distinct features on the graph. The values of the modified Avrami exponent, 'n' and the Tobin exponent, 'n_T' (Table 1) were also found similar and approximately closer to one, which indicated the one dimensional crystals growth [4]. Higher cooling rates provided more number of nucleating sites, and thus facilitating the rate of the crystallization process. The Ozawa plots (Fig. 8b) analyzed at t = 0.01 at 0.8 min gave the perfect fitting ($0.960 \geq R^2 \leq 1.0$) and described the whole crystallization process unlike to other two models that assumed only the low crystalline regions.

A slight nonlinearity of the curves was observed in Ozawa plots at crystallization time, t = 0.01 min that suggested the crystallization behavior in CEM-g-PLA is heterogeneous. At t = 0.2–0.7 min, it showed homogenous behavior but beyond 0.7 min, it again assumed a heterogeneous behavior. Most of the values for the Ozawa exponent, m (Table 1) demonstrated that the crystal growths in CEM-g-PLA were of 1–2 dimensions and were crystallization time dependant.

3.4 The mechanism of the melt crystallization process in CEM-g-PLA

Figure 9a helped to work out the isoconversional activation energy over the fractional area, α value ranging from 0.2 to 0.8. The negative values for the energy confirmed that CEM-g-PLA underwent a typical melt crystallization process. This clear observation agreed to the recent findings on the melt crystallization of polymers [25, 33]. The breakpoints on the E_α versus T plot for CEM-g-PLA (Fig. 9b) indicated a change in the melt crystallization mechanism possibly from heterogeneous to homogenous-like mechanism and vice versa. This abrupt switch in crystallization mechanism has been a known phenomenon as reported in other studies also [34].

4 Conclusion

The thermal degradation behavior of CEM and CEM-g-PLA and melt crystallization kinetics of CEM-g-PLA under non-isothermal conditions were studied in a

Table 1 The modified Avrami, Ozawa, and Tobin crystallization parameters for CEM-g-PLA

Cooling rates (°C/min)	Modified Avrami		Ozawa (t = 0.01–0.8 min)		Tobin	
	n	k_c	m	k	n_T	k_T
10	1.004	0.919	1.121	0.019	1.008	0.433
15	1.042	0.959	1.131	0.050	1.049	0.536
20	1.027	0.977	1.263	0.060	1.037	0.643
			2.113	0.031		
			2.563	0.029		
			2.164	0.069		
			1.698	0.154		
			1.154	0.349		
			0.954	0.510		

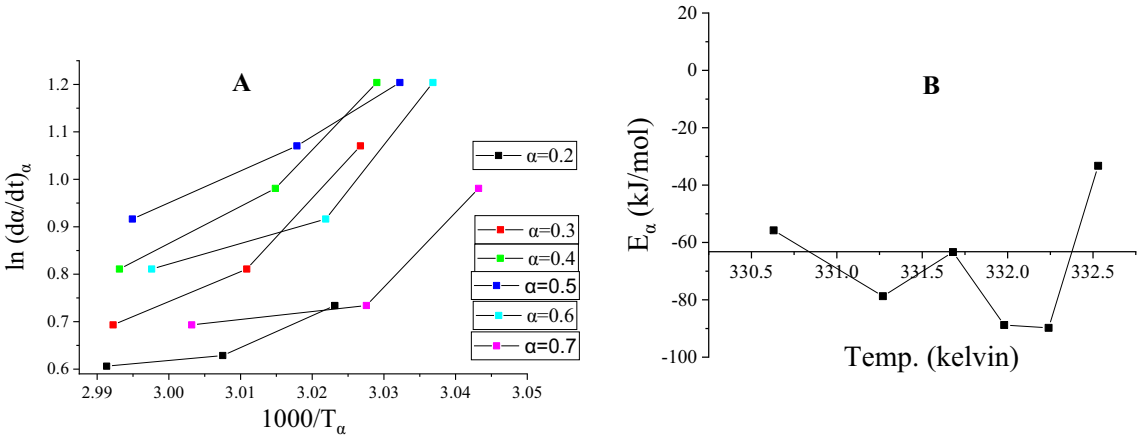

Fig. 9 **a** The isoconversional DSC plots over the fractional area, α = 0.2–0.7 and at the cooling rates 10–20 °C/min and **b** dependence of E_α on T plot. *Note*: The energy term, E_α was determined from the slope of each of the plot (**a**) at the respective α value

comprehensive manner. The CEM-g-PLA followed dimensional diffusions (D1 and D2) and the power laws (P2/3, P2, P3, P4) mechanisms while the CEM showed a number of degradation mechanisms among them were the Mampel first order (F1) and Avrami-Erofeev (A2, A3, A4) mechanisms. The energy profiles obtained from the Friedman method, FWO, and KAS isoconversional models showed variation of E (α) against α that indicated multi-stage thermal degradation kinetics for CEM-g-PLA and the Friedman method for CEM. From the non-isothermal melt crystallization data, in the CEM-g-PLA, primary and secondary crystallization believed to have taken place around the low and high crystalline regions, respectively. The dependence of E_α over T produced from the isoconversional DSC data provided some clue on the melt crystallization mechanism in CEM-g-PLA. Finally, this detailed work would be essential for better understanding the post-PLA grafting effect on the thermal characteristics of mucilagenous polysaccharide like the CEM, which could be used to propose the specific applications of this newer material. It is noteworthy that polylactide-based materials (e.g. PLA, graft copolymer, or their blends) have interesting biomedical and food packaging applications. This analysis might be successfully applied for modeling the degradation stability/mechanism and crystallization characteristic of the green copolymers containing grafted PLA.

Funding Abubakar Hamisu Mijinyawa, sincerely acknowledged the financial support received from the R&D research activities funds, Sharda University, Greater Noida, India (Grant No. SU/2018/428).

Compliance with ethical standards

Conflict of interest There are no conflict to declare.

References

1. Aboulkas A, Harfi KE, Bouadili AE (2010) Thermal degradation behaviors of polyethylene and polypropylene. Part I: pyrolysis kinetics and mechanisms. Energy Convers Manag 51:1363–1369
2. Ahmed J, Varshney SK (2011) Polylactides-chemistry, properties and green packaging technology: a review. Int J Food Prop 14:37–58
3. Akbar J, Iqbal MS, Massey S, Masih R (2012) Kinetics and mechanism of thermal degradation of pentose- and hexose-based carbohydrate polymers. Carbohydr Polym 90:1386–1393
4. Battegazzore D, Bocchini S, Frache A (2011) Crystallization kinetics of poly(lactic acid)-talc composites. eXPRESS Polym Lett 5:849–858
5. Borkotoky SS, Chakraborty G, Katiyar V (2018) Thermal degradation behavior and crystallization kinetics of poly(lactic acid) and cellulose nanocrystals (CNC) based microcellular composite foams. Int J Biol Macromol 118:1518–1531
6. Cazón P, Velazquez G, Ramírez JA, Vázquez M (2017) Polysaccharide-based films and coatings for food packaging: a review. Food Hydrocoll 68:136–148
7. Criado JM (1978) Kinetic analysis of DTG data from master curves. Thermochima Acta 24:186–189
8. Feng L, Feng S, Bian X, Li G, Chen X (2018) Pyrolysis mechanism of poly(lactic acid) for giving lactide under the catalysis of tin. Polym Degrad Stab 157:212–223
9. Filho JGDO, Rodrigues JM, Valadares ACF, Almeida ABD, Lima TMD, Takeuchi KP, Alves CCF, Sousa HADF, Silva ERD, Dyszy FH, Egea MB (2019) Active food packaging: alginate films with cottonseed protein hydrolysates. Food Hydrocoll 92:267–275
10. Friedman HL (1964) Kinetics of thermal degradation of char-forming plastics from thermogravimetry: application to a phenolic plastic. J Polym Sci Chem C Polym Symp Banner 6:183–195
11. Furushima Y, Schick C, Toda A (2018) Crystallization, recrystallization, and melting of polymer crystals on heating and cooling examined with fast scanning calorimetry. Polym Cryst. https://doi.org/10.1002/pcr2.10005
12. Hoffman JD, Davis GT, Lauritzen Jr JI (1976) The rate of crystallization of linear polymers with chain folding. In: Hanny NB (ed). Treatise on solid state chemistry. Springer, Boston, p 497
13. Hua S, Chen F, Liu Z, Yang W, Yang M (2016) Preparation of cellulose-graft-polylactic acid via melt copolycondensation for use in polylactic acid based composites: synthesis, characterization and properties. RSC Adv 6:1973
14. Huang Z, Ye Q, Teng L (2015) A comparison study on thermal decomposition behavior of poly(L-lactide) with different kinetic models. J Therm Anal Calorim 119:2015–2027
15. Iqbal MS, Massey S, Akbar J, Ashraf CM, Masih R (2013) Thermal analysis of some natural polysaccharide materials by isoconversional method. Food Chem 140:178–182
16. Kerrouche D, Sadoun T, Rouba N, Sotclet G, Sol V, Gloaguen V, Chaleix V (2018) Synthesis and characterization of xylan-graft-poly(L-lactide). Int J Polym Anal Charact 23:193–206
17. Koh JJ, Zhang X, He C (2018) Fully biodegradable poly(lactic acid)/starch blend: a review of toughening strategies. Int J Biol Macromol 109:99–113
18. Lizundia E, Vilas JL, Léon LM (2015) Crystallization, structural relaxation and thermal degradation in poly(L-lactide)/cellulose nanocrystal renewable nanocomposites. Carbohydr Polym 123:256–265
19. Luckachan GE, Pillai CKS (2006) Chitosan/oligo L-lactide graft copolymers: effect of hydrophobic side chains on the physicochemical properties and biodegradability. Carbohydr Polym 64:254–266
20. Mabuda AL, Mamphweli NS, Meyer EL (2016) Model free kinetic analysis of biomass/sorbent blends for gasification purposes. Renew Sustain Energy Rev 53:1656–1664
21. Malkappa K, Bandyopadhyay J, Ray SS (2018) Thermal degradation characteristic and flame retardancy of polylactide-based nanobiocomposites. Molecules 23:2648
22. Mijinyawa AH, Durga G, Mishra A (2018) Isolation, characterization, and microwave assisted surface modification of *Colocasia esculenta* (L.) Schott mucilage by grafting polylactide. Int J Biol Macromol 119:1090–1097
23. Mishra G, Bhaskar T (2014) Non-isothermal model free kinetics for pyrolysis of rice straw. Bioresour Technol 169:614–621
24. Mothe CG, Freitas JS (2018) Lifetime prediction and kinetic parameters of thermal decomposition of cashew gum by thermal analysis. J Therm Anal Calorim 131:397–404
25. Pin JM, Mija A, Sbirrazzuoli N (2017) Stereodynamic control of star-epoxy/anhydride crosslinking actuated by liquid-crystalline phase transitions. Soft Matter 13:1956–1965

26. Salimi K, Topuzogullari M, Dincer S, Aydin HM, Piskin E (2016) Microwave-assisted green approach for graft copolymerization of l-lactic acid onto starch. J Appl Polym Sci 133:42937–42944
27. Salimi K, Yilmaza M, Rzayeva ZMO, Piskin E (2014) Controlled graft copolymerization of lactic acid onto starch in a supercritical carbon dioxide medium. Carbohydr Polym 114:149–156
28. Sarkar G, Saha NR, Roy I, Bhattacharyya A, Bose M, Mishra R, Rana D, Bhattacharjee D, Chattopadhyay D (2014) Taro corms mucilage/HPMC based transdermal patch: an efficient device for delivery of diltiazem hydrochloride. Int J Biol Macromol 66:158–165
29. Sattari M, Mirsalehi SA, Khavandi A, Alizadeh O, Naimi-Jamal MR (2015) Non-isothermal melting and crystallization behavior of UHMWPE/SCF/nano-SiO_2 hybrid composites. J Therm Anal Calorim. https://doi.org/10.1007/s10973-015-5003-4
30. Sergey V, Alan KB, José MC, Luis AP, Crisan P, Nicolas S (2011) The ICTAC Kinetics Committee recommendations for performing kinetic computations on thermal analysis data. Thermochim Acta 520:1–19
31. Singh V, Kumar P, Sanghi R (2012) Use of microwave irradiation in the grafting modification of the polysaccharides-A review. Prog Polym Sci 37:340–364
32. Vyazovkin S (2006) Thermal analysis. Anal Chem 78:3875–3886
33. Vyazovkin S (2018) Modern isoconversional kinetics: from misconceptions to advances. In: Vyazovkin S, Koga N, Schick C (eds) Handbook of thermal analysis and calorimetry, vol 6. Elsevier, Amsterdam, pp 131–172
34. Vyazovkin S (2018) Nonisothermal crystallization of polymers: getting more out of kinetic analysis of differential scanning calorimetry data. Polym Cryst 1:1–6
35. White JE, Catallo WJ, Legendre BL (2011) Biomass pyrolysis kinetics: a comparative critical review with relevant agricultural residue case studies. J Anal Appl Pyrol 91:1–33
36. Wu Y, Zheng Y, Yang W, Wang C, Hu J, Fu S (2005) Synthesis and characterization of a novel amphiphilic chitosan–polylactide graft copolymer. Carbohydr Polym 59:165–171
37. Yang J, Xu Y, Nie S, Cheng G, Tao Y, Zhu J (2018) Morphological structure, impact toughness, thermal property and kinetic analysis on the cold crystallization of poly(lactic acid) biocomposites toughened by precipitated barium sulfate. Polym Degrad Stab 158:176–189

Publisher's Note Springer Nature remains neutral with regard to jurisdictional claims in published maps and institutional affiliations.